AFRL-AFOSR-VA-TR-2024-0047

Lasing in 2D Group IV Nanomaterials

Panthani, Matthew
IOWA STATE UNIVERSITY
1350 BEARDSHEAR HALL
AMES, IA,
US

11/30/2023
Final Technical Report

Air Force Research Laboratory
Air Force Office of Scientific Research
Arlington, Virginia 22203
Air Force Materiel Command

REPORT DOCUMENTATION PAGE

PLEASE DO NOT RETURN YOUR FORM TO THE ABOVE ORGANIZATION.

1. REPORT DATE	2. REPORT TYPE	3. DATES COVERED	
20231130	Final	START DATE 20200701	END DATE 20230630

4. TITLE AND SUBTITLE
Lasing in 2D Group IV Nanomaterials

5a. CONTRACT NUMBER	5b. GRANT NUMBER	5c. PROGRAM ELEMENT NUMBER
	FA9550-20-1-0018	61102F
5d. PROJECT NUMBER	**5e. TASK NUMBER**	**5f. WORK UNIT NUMBER**

6. AUTHOR(S)
Matthew Panthani

7. PERFORMING ORGANIZATION NAME(S) AND ADDRESS(ES)
IOWA STATE UNIVERSITY
1350 BEARDSHEAR HALL
AMES, IA
US

8. PERFORMING ORGANIZATION REPORT NUMBER

9. SPONSORING/MONITORING AGENCY NAME(S) AND ADDRESS(ES)	10. SPONSOR/MONITOR'S ACRONYM(S)	11. SPONSOR/MONITOR'S REPORT NUMBER(S)
Air Force Office of Scientific Research 875 N. Randolph St. Room 3112 Arlington, VA 22203	AFRL/AFOSR RTB1	AFRL-AFOSR-VA-TR-2024-0047

12. DISTRIBUTION/AVAILABILITY STATEMENT
A Distribution Unlimited: PB Public Release

13. SUPPLEMENTARY NOTES

14. ABSTRACT
Reports of lasing in Group IV semiconductors have required high optical pumping energies due to a preference for non-radiative charge carrier recombination pathways. We proposed a completely different approach – using 2D Group IV materials that have direct band gaps and have demonstrated strong light emission. Thus, these materials are expected to exhibit low lasing thresholds. This will be highly important to the broad scientific community and advance the chemistry of materials that can benefit DoD capabilities in communication, surveillance, and computing. In the second year of this project, our research group has made progress in understanding structure-property relationships in 2D Group IV semiconductors that can become the basis of future optoelectronic devices. In the final year of this project, we report two major findings: (1) the synthesis of GeSn nanosheets with 50 at % Sn and mid-infrared absorbance, and (2) demonstrating optical gain in Si nanosheets by using surface chemistry to engineer their band structures.

15. SUBJECT TERMS

16. SECURITY CLASSIFICATION OF:			17. LIMITATION OF ABSTRACT	18. NUMBER OF PAGES
a. REPORT U	b. ABSTRACT U	c. THIS PAGE U	UU	16

19a. NAME OF RESPONSIBLE PERSON	19b. PHONE NUMBER *(Include area code)*
GERNOT POMRENKE	426-8426

Standard Form 298 (Rev.5/2020)
Prescribed by ANSI Std. Z39.18

Lasing in 2D Group IV Nanomaterials
Project Report

Award Number: *FA9550-20-1-0018*

Report type: *Final Report*

Reporting Period: 01 Jul 20 – 31 Jun 23

Program Office Name: Dr. Gernot Pomrenke

Project Title: Lasing in 2D Group IV Nanomaterials

Abstract. Reports of lasing in Group IV semiconductors have required high optical pumping energies due to a preference for non-radiative charge carrier recombination pathways. We proposed a completely different approach – using 2D Group IV materials that have *direct band gaps* and have demonstrated strong light emission. Thus, these materials are *expected* to exhibit low lasing thresholds. This will be highly important to the broad scientific community and advance the chemistry of materials that can benefit DoD capabilities in communication, surveillance, and computing. In the second year of this project, our research group has made progress in understanding structure-property relationships in 2D Group IV semiconductors that can become the basis of future optoelectronic devices. In the final year of this project, we report two major findings: (1) the synthesis of GeSn nanosheets with 50 at % Sn and mid-infrared absorbance, and (2) demonstrating optical gain in Si nanosheets by using surface chemistry to engineer their band structures.

A. Participants

Principal Investigator: Matthew G. Panthani, Associate Professor of Chemical and Biological Engineering, Iowa State University

Other Personnel:

Funded students and postdoctoral fellows

- Dr. Jeremy Essner, Postdoctoral Associate, Chemical Engineering, Iowa State University
- Dr. Abhijit Bera, Postdoctoral Associate, Chemical Engineering, Iowa State University
- Bradley J. Ryan, PhD 2022, Chemical Engineering, Iowa State University
  - *Current position: Inpria Corp*
- Atefe Hadi, PhD 2021, Chemical Engineering, Iowa State University
  - *Current position: Intel Corp*
- Carly Dolgos, M.S. 2021
- Maharram Jabrayilov, PhD student (2023 – present)
- Abhishek Chaudhary, PhD student (2023 – present)

Other Partners and Collaborators

Ames National Laboratory – Matthew Besser

Access to materials characterization facilities

Argonne National Laboratory – Benjamin Diroll, Xuedan Ma

Access to spectroscopic equipment, magnetic field-dependent photoluminescence, optically detected magnetic resonance (ODMR)

B. Results and Accomplishments

Overall Objective: Synthesize brightly emitting 2D Group IV semiconductors (comprised of Si, Ge, and Sn) and demonstrate optically pumped amplified stimulated emission (lasing).

Results from funding

Achieving control over structure, defects, and passivation is essential for controlling materials' optical and optoelectronic properties. In Group IV materials, light emission is challenging due its indirect bandgap. However, quantum confinement and surface effects enable new paths for creating light-emitting structures from Group IV semiconductors. This year's progress focused on understanding and controlling structure and defects and their impact on electronic band structure. In this year, key accomplishments include:

1. **New insight** into the structure and stability of 2D Group IV nanostructures using pair distribution function analysis, solid state NMR, and other spectroscopic tools.
2. **Transport properties** of 2D Ge.
3. **Evidence of direct bandgap transitions** in 2D Si by controlling surface chemistry
4. **Synthetic studies** demonstrating a path to 2D GeSn with 50% Sn content.
5. **Investigation of Lasing** demonstrating optical gain in 2D Ge.

1. New Insight into structure and stability

We previously determined that the local bonding and coordination of 2D Si is best described with an atomically thin layer of hexagonally arranged Si atoms, with each Si atom connected to three other Si atoms and predominantly one hydrogen atom. Here, we sought to further elucidate the structure of 2D Si using atomic PDF analysis. While conventional X-ray diffraction (XRD) uses Bragg diffraction to characterize long-range periodicity, PDF uses total X-ray scattering to characterize structures that may not be periodic over long-length scales.

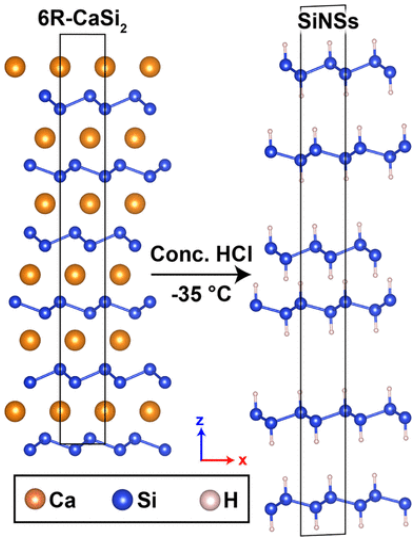

Figure 1. *Schematic showing the 6R phase of $CaSi_2$ (left) and the refined structure of the 2D Si(right). The locations of the hydrogen atoms were determined by density functional theory (DFT). The black box corresponds to the unit cell.*

The 2D Si product obtained from deintercalation is a yellow fluffy powder whose volume is ~150% of the volume of the $CaSi_2$ precursor. The product is not in the form of cohesive crystallites, bringing into question the stacking sequence and registry of adjacent sheets within stacks of 2D Si. The stacking sequence within disordered stacks of 2D Si has not been studied in the literature, which motivates performing structural refinement to elucidate the long-range structure. During the structural refinement process, we investigated several degrees of freedom, including the number of sheets within a unit cell, the spacing between sheets, the

relative translational and rotational alignment of each sheet within the unit cell, and location of each atom within each sheet (**Figure 1**).

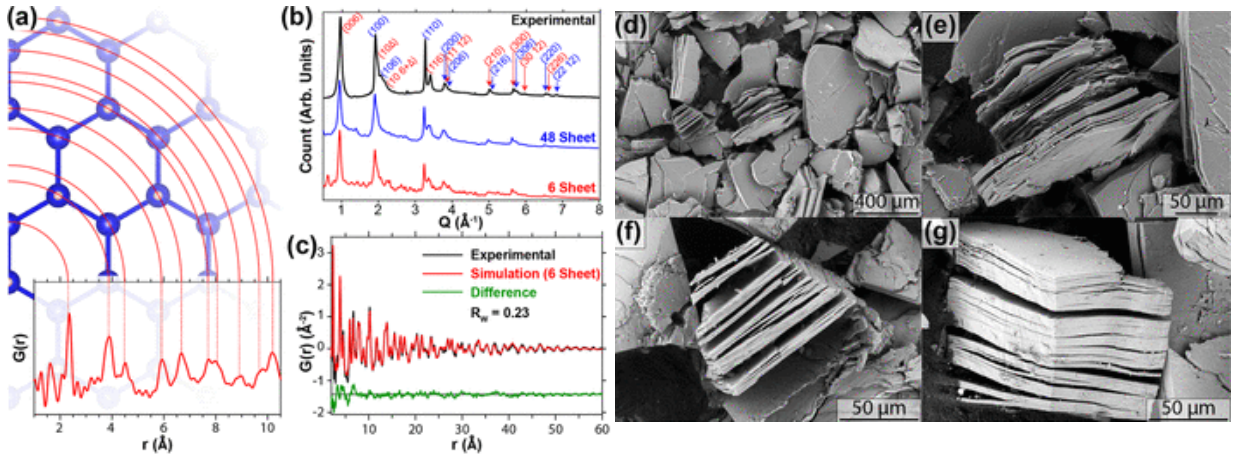

Figure 2. Structural Model of layered 2D Si. ***(a)*** *Schematic of a single SiNS centered about an arbitrary Si atom, demonstrating each neighbor mapping onto each experimental PDF peak.* ***(b)*** *AI-spXRD of the experimental sample (top, black) and the simulated pXRD pattern for the refined structures (bottom, blue and red). The red and blue Miller indices are to help with differentiation. At Q = ~2 Å–1, Δ is an integer such that 1 ≤ Δ ≤ 5.* ***(c)*** *Experimental PDF (black) and the refined 6-sheet structure (red) with the difference curve offset below (green). The AI-spXRD past Q = ~6 Å–1 shows an artificial decrease in intensity due to the edges of the detector.* ***(d–g)*** *SEM images of deintercalated 2D Si.*

The refined structure consists of six 2D Si within a unit cell (**Figure 1**); however, we note that many peaks within the PDF align with a unit cell consisting of a single isolated SiNS without neighboring sheets (**Figure 2a**), albeit with a poor overall fit. This suggests that the features in PDF that are not captured by a single nanosheet are a result of small perturbations in the intersheet spacing of adjacent 2D Si along the c-axis. This is further supported by the broad (006) peak relative to the (110) and (100) peaks in the azimuthally integrated synchrotron powder X-ray diffraction data (AI-spXRD) (**Figure 2b**). Further, we simulated the powder X-ray diffraction (pXRD) pattern of the refined structure containing six sheets per cell (**Figure 2b**), and upon comparing the simulated pXRD pattern to the AI-spXRD, we find that all of the low-intensity peaks in the simulated pXRD with $Q < \sim 1$ Å^{-1} correspond to lower-order (00*l*) peaks (with $l < 6$) that are not observed in the experimental data. These peaks with $Q < \sim 1$ Å^{-1} correspond to the mth nearest neighboring sheets, for $m \geq 2$ (note that $m = n + 1 - 1$, for a unit cell containing n sheets). This indicates that stacking of individual 2D Si within the structure is not periodic. Rather, the lack of features at $Q < \sim 1$ Å^{-1} and the broad (006) peak indicate a broad distribution of intersheet spacings centered at about 6.48 Å. To better model the intersheet disorder, we considered unit cells containing integer multiples of six sheets per unit cell (i.e., 12, 18, 24, ..., 48 sheets per unit cell) that again retain the same x- and y-coordinates and stacking sequence as 6R-$CaSi_2$, but the intersheet spacings were refined to the experimental PDF data. We find that the peaks at $Q < \sim 1$ Å^{-1} in the simulated pXRD are suppressed when modeling these larger unit cells (**Figure 2b**); this supports that the peaks at $Q < \sim 1$ Å^{-1} in the simulated pXRD emerge from the periodicity of the simulated unit cell and are a result of modeling a disordered

system with a periodic unit cell. In addition, the small, low-intensity ripples in the simulated pXRD (e.g., Q in the ranges of *ca.* 1.2–1.8, 2.5–3.2, and 4.0–4.9 $Å^{-1}$) are also suppressed when including increased sheets per unit cell (**Figure 2b**), as these peaks also correspond to the periodicity of mth nearest neighboring sheets (for $m \geq 2$) in the periodic unit cell.

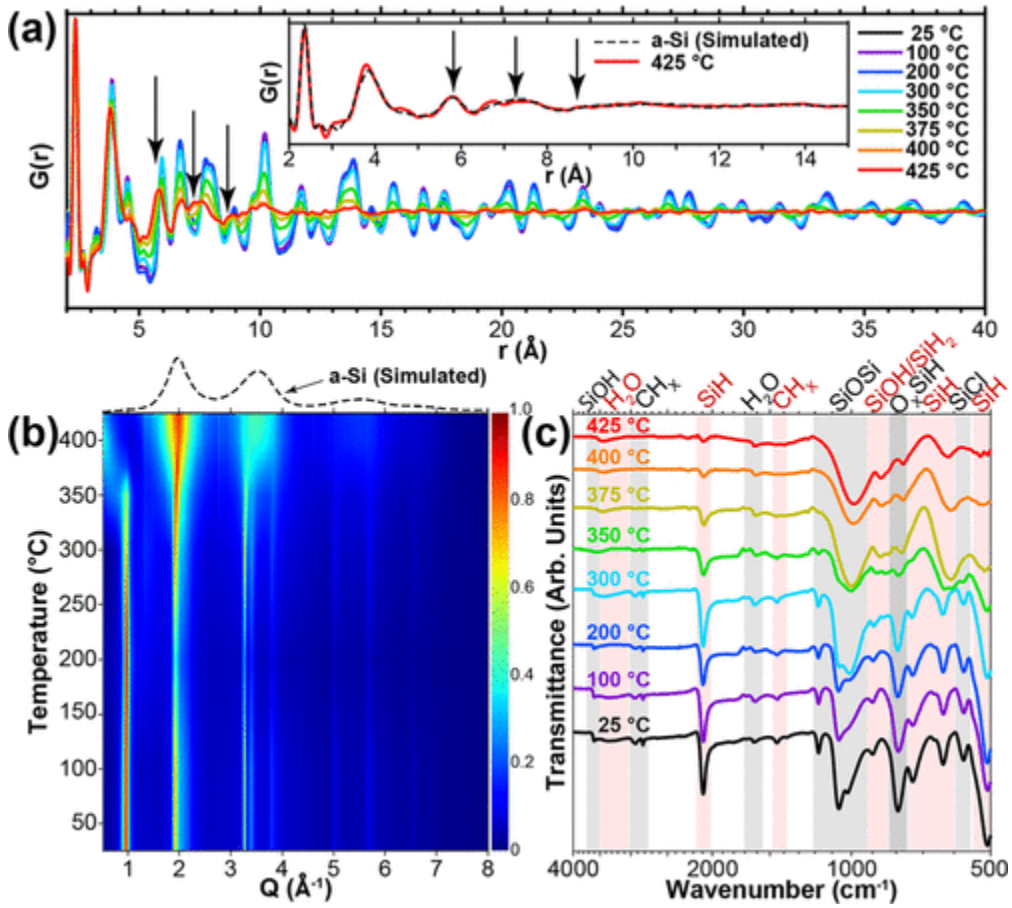

Figure 3. Structural and chemical properties of annealed 2D Si. All data were collected at room temperature. (a) *PDF of 2D Si annealed at different temperatures. Inset is the PDF of the sample annealed at 425 °C and a simulation of the PDF of amorphous Si.* ***(b)*** *AI-spXRD mapped over annealing temperatures. Above the figure (black dashed line) is a simulation of pXRD of a-Si.* ***(c)*** *FTIR of annealed 2D Si; note that the x-axis is on a logarithmic scale. Vertical red and gray bands are to guide the eye. The assignments on the top of the figure correspond to the unannealed sample (25 °C).*

The 2D Si was annealed at different temperatures in a glovebox filled with nitrogen (N_2), cooled to room temperature, and sealed in capillaries under an Ar atmosphere. X-ray scattering was measured at Argonne National Laboratory Advanced Photon Source (APS), beamline 11-ID-B. The PDF and AI-spXRD of the annealed 2D Si are shown in **Figure 3**. The PDF and AI-spXRD change very little up to 300 °C, but a broadening of all the peaks in the AI-spXRD begins between 300 and 350 °C (**Figure 3b**). This broadening continues to increase to 425 °C, whereupon the resulting AI-spXRD resembles that of amorphous Si (a-Si). In this temperature range, all PDF peaks that correspond to the 2D Si begin to decrease in intensity, while the

systematic absences in the 2D Si that occur in 3D bulk c-Si begin to increase in intensity (black arrows in **Figure 3a**). At 425 °C the PDF resembles that of a-Si, indicating that the 2D framework begins to form additional bonds along the c-axis. However, the slight deviation in the peak locations after annealing at 425 °C indicates that the transformation into a-Si is not complete, and additional Si–Si bonds would continue to form at temperatures of >425 °C; this hypothesis is later probed with UV–vis. Further, upon inspecting the PDF and AI-spXRD at 425 °C, the resemblance to a-Si becomes apparent. Indeed, the PDF and AI-spXRD both suggest that the 2D Si undergo structural amorphization to a-Si beginning at temperatures near 300 °C; this is done so by forming Si–Si bonds in the third dimension. We have begun neutron scattering and solid-state NMR to characterize lighter elements (oxygen, hydrogen, chlorine) that cannot be probed using x-rays. Finalizing these results will be a focus in the final year of this project.

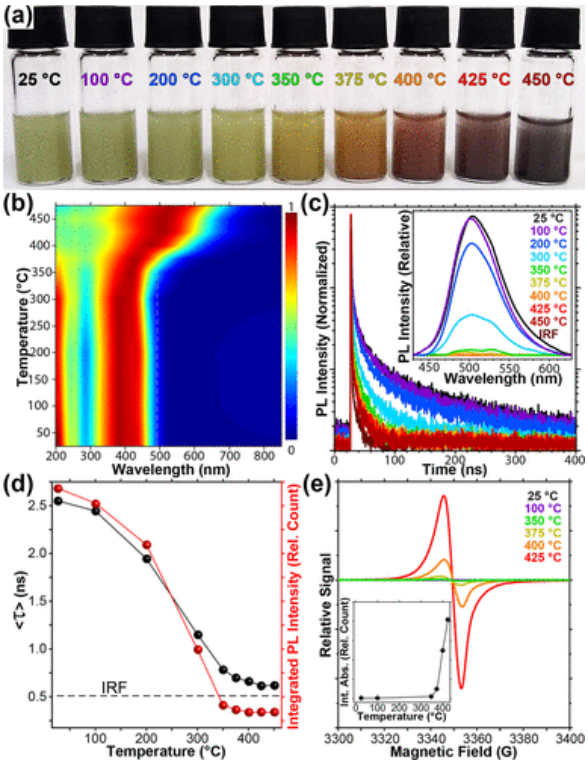

Figure 4. Optical properties of annealed 2D Si. (a) *Photograph of the annealed samples dispersed in methanol at 3 mg/mL.* ***(b)*** *Heat map of the Kubelka–Munk transformation of diffuse reflectance spectra;* ***(c)*** *Time-resolved photoluminescence of annealed;inset is the corresponding steady-state photoluminescence.* ***(d)*** *Average photoluminescence lifetime (left, black axis) and total integrated photoluminescence intensity (right, red axis). Horizontal dashed line corresponds to the IRF lifetime.* ***(e)*** *Electron paramagnetic resonance of annealed 2D Si*

To quantify the visible changes in color that occurred upon annealing the 2D Si, we collected diffuse reflectance data and used the Kubelka–Munk (KM) function to transform these data into pseudoabsorbance (**Figure 4b**). Similar to the FTIR data above, we observe no appreciable difference in the KM line shape up to 200 °C. However, at 300 °C, there is a blue-shift in the onset of absorption from its value of ~501 nm (2.48 eV) at 25 °C to ~486 nm (2.55 eV) at 300 °C, but this blue-shift is then reversed back to its initial onset of absorption by 350 °C. We would like to point out that this blue-shift is reproducible and has been reported before in the literature in studies of "siloxene". This blue-shift could be due to chemical reactions with water or trace O_2 within the N_2-filled glovebox or the insertion or rearrangement of the oxygen of SiOH into Si–Si bonds. Given that the DFT results presented above indicate that the formation of SiOSi is more favorable than the formation of SiOH, we suspect that such a reaction with water or O_2 would yield O_x–Si–Si_{3-x} bonds. At temperatures greater than 350 °C, the onset of absorption begins to shift toward the red. We attribute this red-shift to the structural disorder and consequently a distribution of allowed optical transitions with energies less than that of the unannealed 2D Si. By 475 °C, the onset of absorption occurs near 1.65 eV, consistent with a-Si.

In summary, we used synchrotron X-ray diffraction, neutron scattering, atomic pair distribution function (PDF) analysis, and a variety of spectroscopic techniques to characterize the structure and thermal stability of 2D Si. We found that 2D Si exhibits disorder within the intersheet spacing, but have little translational or rotational disorder among adjacent 2D Si sheets. Furthermore, we identify changes in their structural, chemical, and optical properties after being heated in an inert atmosphere up to 475 °C. We characterized changes of the annealed 2D Si using synchrotron-based total X-ray scattering, infrared spectroscopy, X-ray photoelectron spectroscopy, scanning electron microscopy, electron paramagnetic resonance, absorbance, photoluminescence, and excited-state lifetime. The silicon framework is robust, with an onset of amorphization at ~300 °C, which is well above the required operating temperatures of photonic devices. Above ~300 °C, we demonstrate that the 2D Si begin to coalesce while keeping their translational alignment to yield amorphous silicon nanosheets. In addition, our DFT results provide information on the structure, energetics, band structures, and vibrational properties of 11 distinct oxygen-containing nanosheets. Overall, these results provide critical information for the implementation of atomically thin silicon nanosheets in next-generation CMOS-compatible integrated photonic devices.

2. Transport Studies in 2D Germanium

2D Ge has been of interest due to experimental and theoretical evidence of high charge carrier mobilities exceeding 10,000 $cm^2\ V^{-1}\ s^{-1}$.

In collaboration with researchers at Université de Lille and Université de Sorbonne, we investigated transport properties of 2D Ge using. Methyl-terminated 2D Ge ("methyl-terminated germanane") microcrystallites were first examined with the UHV-SEM of the nanoprobe system. Prior to their observation, they were annealed for 3 h in the UHV preparation chamber to remove adsorbed impurities. The microcrystallites were electrically characterized with multiple-tip STM. Moreover, when contact is achieved, due to their partial oxidation, the insulating character of these microcrystallites results in highly resistive contacts which preclude the injection of current into the microcrystallites. Conversely, on the well-resolved microcrystallites (**Figure 5**), the I-V characteristics were linear as shown in **Figure 5c**. Analyzing the resistance as a function of tip separation revealed two types of behavior among these microcrystallites:

(1) For microcrystallites where the separation of the tips is in the range of the microcrystallite thickness, the resistance increases with the tip spacing. For example, the microcrystallite seen in **Figure 5a** has an electrical resistance that linearly increases for more than 4 kΩ, when the tip separation varies between 0.7 μm and 2.5 μm (**Figure 5d**). Due to a crystallite thickness which is smaller than the outer tip separation, the current distribution is compressed at the bottom of the crystallite, raising its electrical resistance (**Figure 5b**).
(2) Conversely, for thicker microcrystallites where the tip separation is smaller than the microcrystallite thickness, the current predominantly flows near the surface. Hence, the resistance is inversely proportional to the distance between the tips. Such an example is illustrated in **Figure 5f** (for the microcrystallite observed in **Figure 5e**).

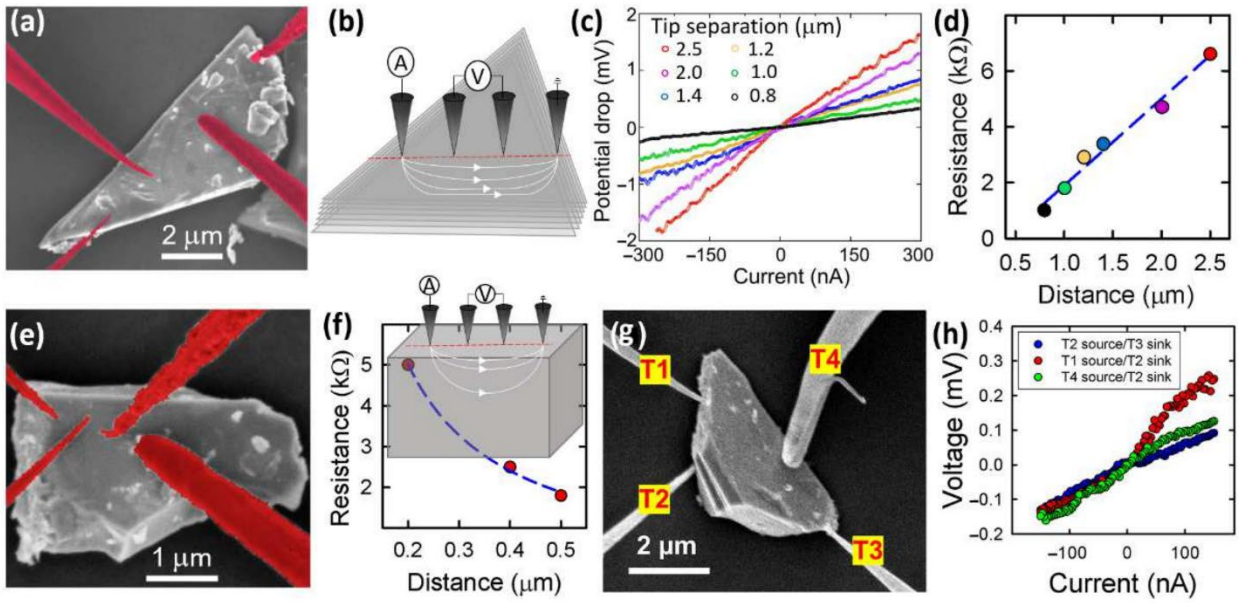

Figure 5. ***(a)*** *SEM image of a methyl-terminated germanane microcrystallite contacted with four STM tips. The STM tips have been colorized to be better differentiated from the crystallite.* ***(b)*** *Schematic of the current flow with a compressed current distribution due to the limited thickness of the crystallite.* ***(c)*** *V(I) characteristics measured for six different equidistant tip separations.* ***(d)*** *Linear variation of the four-point resistance as a function of the probe separation. The dashed line corresponds to the best fit.* ***(e)*** *SEM image of a methyl-terminated germanane microcrystallite contacted with four STM tips and* ***(f)*** *related four-point resistance. The dashed line corresponds to the best fit, which is inversely proportional to the equidistant probe spacing. Inset: Schematic illustration of the current flow pattern for a thick microcrystallite.* ***(g)*** *SEM image of a methyl-terminated germanane microcrystallite contacted with STM tips from different facets and* ***(h)*** *corresponding four-point resistances as a function of the position of the source tip and the grounded tip.*

While strikingly different, both behaviors are consistent with a three-dimensional transport. At small tip distances, despite the finite size of the microcrystallite, the four-point resistance verifies Ohm's law for a homogeneous and isotropic semi-infinite three-dimensional resistive material, $R_{4p} = \rho_{3D}/2\pi d$, where ρ_{3D} and d are the bulk resistivity of the microcrystallite and the tip separation, respectively. At larger distances, the four-point resistance verifies the relationship $R_{4p} = \rho_{3D}d/S$, where S is the cross-sectional area of the microcrystallite. Confirmation of three-dimensional transport is provided by changing the probe arrangement. Instead of contacting the same top plane, the source tip can be in contact with an edge facet and the potential probes positioned across the microcrystallite as the electrodes for the source. Ground and potential detection are then easily commutable. Such a situation is illustrated in **Figure 5g**. This might give rise to slight deviation on the V(I) characteristics due to small changes in the injection of electrons when the tip sourcing of the current is in contact with rough facets. Overall, however, the V(I) curves yield resistances around 1 kΩ (**Figure 5h**), which is in agreement with the resistances found before. Although the microcrystallites can be seen as parallel resistors, their manipulation with the STM tips reveal a defective layered morphology, as shown in the SEM side views of Figure 1c. This inhomogeneous structure, with a random presence of dislocations

and grain boundaries, renders the estimation of the resistivity of a single methyl-terminated germanane layer impossible.

We compare the resistance of methyl-terminated germanane microcrystallites with the resistance of H-terminated germanane flakes found in the literature. Although the H-terminated germanane flakes show similar lateral sizes, they were much thinner. Hence, we normalized the resistance by multiplying it by the measured thickness of the microcrystallite. For annealing temperature around 180 °C, the electrical measurements show similar results between the CH_3-terminated microcrystallites and the H-terminated flakes. At a temperature of 210 °C, the resistance of the H-terminated germanane flakes strongly decreases, whereas annealing the methyl-terminated germanane microcrystallites at 280 °C for 12 h does not lead to any significant change in resistance. The stability of the electrical conduction at varying temperatures is supported by the structural analysis of the microcrystallites. The resistivity of H-terminated germanane drops after an annealing at 210 °C, presumably due to hydrogen desorption and the possible transformation of the layers into *germanene* layers. In contrast, the Ge—C bonds are stronger and more resistant to oxidation. The stronger surface passivation leading to greater thermal stability, which explains the difference between our results and prior results on H-terminated germanane.

In summary, we performed transport measurements on methyl-terminated 2D Ge flakes and found that their electronic properties are similar to those reported by others in H-terminated Ge, but with greater thermal stability. We found the electronic properties are dependent on adsorbed moisture. The impressive stability, combined with their potential for high mobility (>10^4 cm^2 V^{-1} s^{-1}) makes 2D Ge a promising candidate for a high-mobility 2D material that is compatible with CMOS and backend-of-the-line processes.

3. Evidence of Direct Bandgap Transitions in 2D Si

One approach for band structure engineering in these materials is through controlled chemical (i.e., structural, surface) modification. To achieve this, a more comprehensive understanding of the native material structure and its (surface) reactivity are required. Towards this, we exposed 2D Si to increasing quantities of

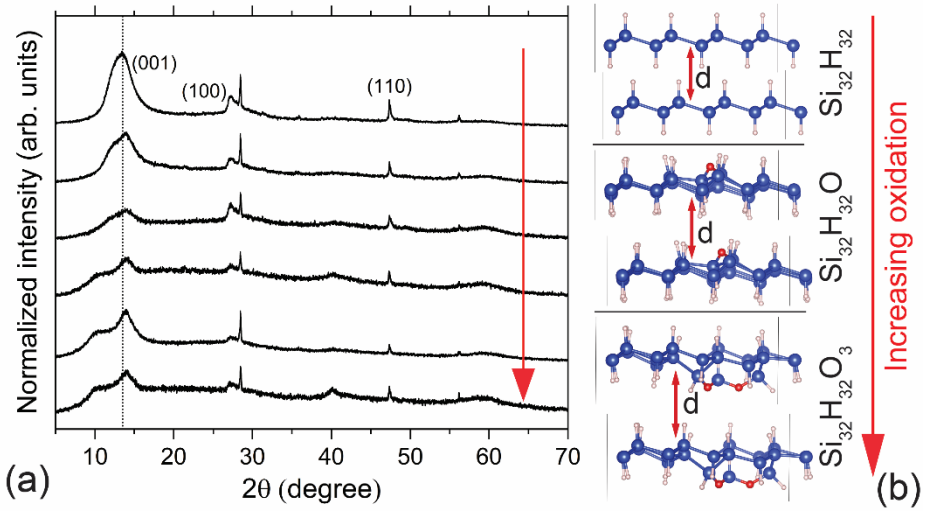

Figure 6. (a) *pXRD patterns of 2D Si exposed to increasing quantities of oxygen (indicated by red arrow).* ***(b)*** *DFT simulated 2D Si structures with increasing quantities of inserted oxygen, highlighting the structural buckling and increase in interlayer spacing.*

dry air, as our band structure simulations demonstrate that oxidation of the material leads to a direct bandgap of lower energy (2.19 eV to 2.11 eV) over a non-oxidized material (**Figure 7c**). pXRD measurements revealed that exposure to increasing quantities of oxygen (O_2) led to the emergence of bimodal diffraction associated with the interlayer nanosheet spacing ($2\theta \approx 13.5°$; (001) peak), which eventually separate into two distinct peaks centered at $2\theta \approx 10°$ and $2\theta \approx 14°$ (**Figure 6a**). These results indicate increasing disorder in the 2D Si structure with the interlayer spacing both increasing and decreasing, respectively. DFT simulations predict that insertion of oxygen in the 2D Si backbone induces structural strain that further buckles the Si network, impacting atomic configurations over five Si sites away for just one in 32 Si atoms oxidized to O_xSiH (**Figure 6b**). This structural buckling will push the SiNSs apart in areas of oxidation with non-oxidized areas being slightly forced together from the induced strain on the backbone structure. Such a scenario accounts for the larger shift in 2θ from 13.5° to 10° for increasing interlayer d spacing, while only a marginal shift of approximately 0.5° is observed for the decreasing interlayer spacing.

To further corroborate that air exposure led to oxygen insertion, the 2D Si was characterized with FTIR. In general, the FTIR spectral profiles are consistent with previous samples generated in our lab, where the 2D Si surface is comprised of -H, -OH, and -Cl functionalities. Such assignments are supported by DFT simulations (not shown). With increasing oxygen exposure, the following changes to vibrations associated with Si-O bonds are observed (**Figure 7a**): (i) the asymmetric stretch of Si-O-Si (~1050 cm^{-1}) markedly increases, two peaks between 810-910 cm^{-1} from O_xSiH bending grown in, and a weak peak near 2250 cm^{-1} from Si-H stretching of O_3SiH emerges, all indicating oxidation of the Si network via insertion of oxygen. Consistent with DFT predictions, increasing levels of oxidation increase the photoluminescence of the material along with a bathochromic shift in peak emission, indicating the oxidized material possesses more direct character with a lower bandgap (**Figure 7b**). Another noteworthy outcome of these studies was the development of synthetic

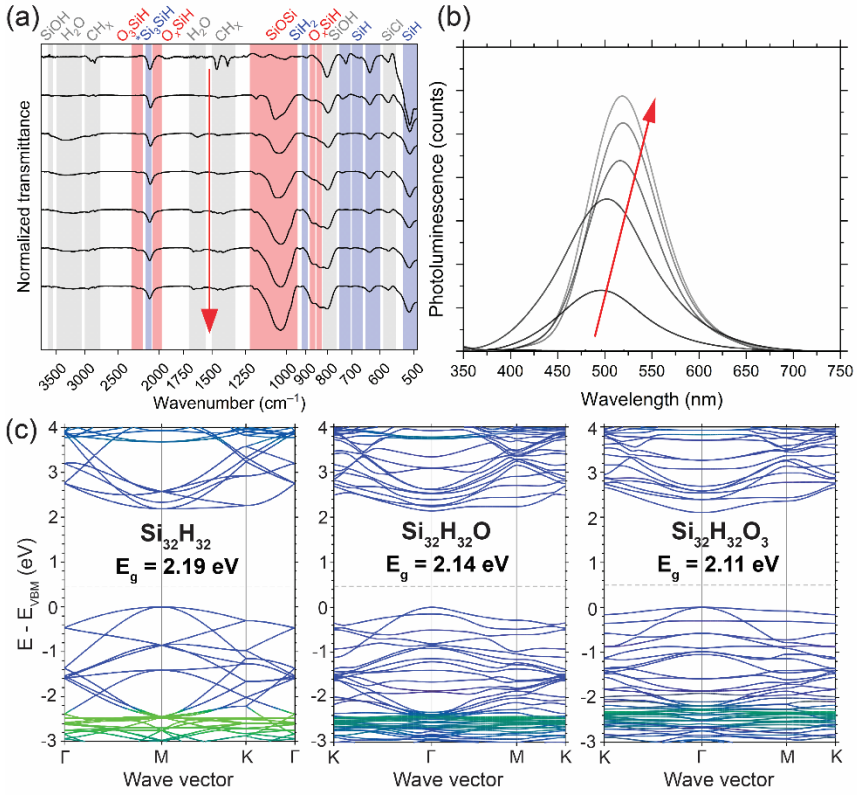

Figure 7. *(**a**) FTIR and (**b**) photoluminescence spectra of 2D Si exposed to increasing quantities of oxygen (indicated by red arrows). (**c**) Simulated band structures for fully hydrogen terminated 2D Si (left) with one (middle) and three (right) inserted oxygen atoms in the form of Si-O-Si.*

conditions that yield 2D Si free of oxidation (as assessed by FTIR), a material that displays essentially zero quantifiable emission and possesses a structure closer to "silicane" than any other reported works. Furthermore, the results reveal that the commonly reported, effectively "off/on" emission for this material finds its origins in oxidation of the Si layer, likely arising from chemical confinement of $(SiH)_y$ within oxidized "islands" (e.g., $(O_xSiH)_z$). Again, such luminescent behavior is consistent with our band structure predictions. In addition to arriving at 2D Si with a direct bandgap, the conclusions drawn from these studies add to the growing "library" of structure-property relationships for this material.

In an alternate avenue for band structure engineering, we deintercalated the $CaSi_2$ precursor with increasing quantities of dissolved $Cl_2(g)$ instead of the conventional aqueous HCl, operating under the hypothesis that such conditions would lead to chlorine terminated 2D Si. Consistent with termination by a larger atom (i.e., Cl), the pXRD patterns of the resulting 2D Si material show increased interlayer spacing relative to hydrogen terminated 2D Si (**Figure 8a**). Furthermore, with increasing quantities of chlorine, the structure becomes more disordered, evidenced by the decrease and loss of intensity for the (001) and (100) peaks, respectively. Most noteworthy, is the marked increase in photoluminescence with increasing quantities of chlorine (**Figure 8b**), with the highest quantum yield being nearly thrice that of hydrogen-terminated 2D Si (<9% vs. 24%). Additionally, the emission is slightly red shifted relative to hydrogen-terminated 2D Si. These PL results are indicative of a transition to a direct band structure with a lower bandgap. Tentatively, the above results are attributed to chlorine functionalization, however, an alternate hypothesis is that the material is functionalized with methoxy groups due to reaction with methanol; material characterization is still ongoing. Regardless, this approach yields a brightly emitting Group IV material that should show promise in optoelectronics and lasing.

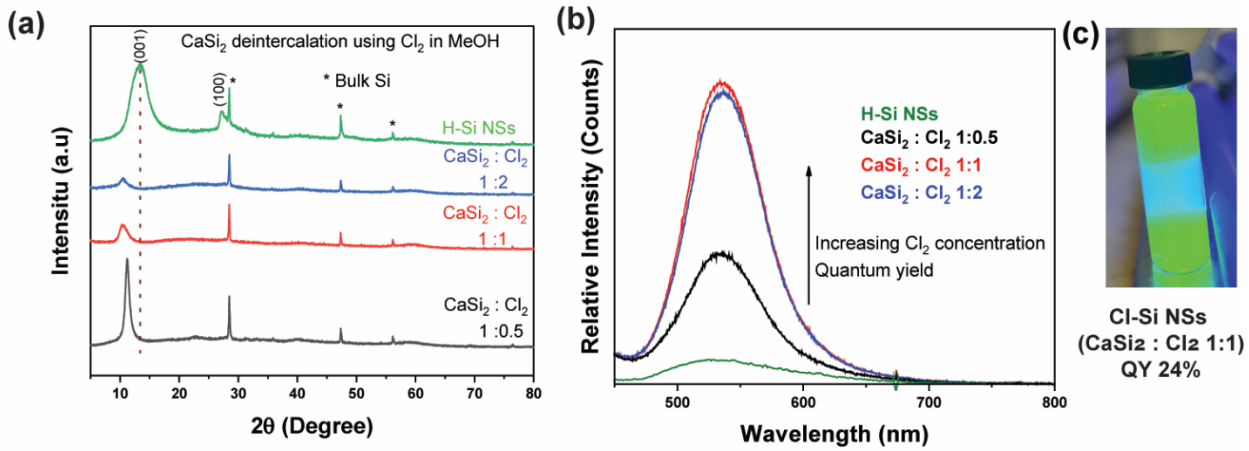

Figure 8. ***(a)*** *pXRD of materials generated by deintercalating $CaSi_2$ with increasing quantities of Cl_2 in methanol (MeOH). The pXRD pattern of hydrogen terminated Si nanosheets (H-Si NSs) is provided for reference. Note, the values of $CaSi_2$:Cl_2 are mole ratios.* ***(b)*** *Photoluminescence spectra of these same materials.* ***(c)*** *Representative picture of the brightly green emitting material is shown on the right.*

In summary, by controlling interfacial chemistry, we engineered the electronic band structure of 2D Group IV materials to create highly emissive materials with evidence of a direct bandgap. In route to this, we found synthetic conditions that yield 2D Si with the closest structure to "silicane" that has been reported, which adds further understanding to the structure-property relationships of this material. We experimentally engineered the band structure, with the support of DFT simulations, to yield highly emissive 2D Si, with the chlorine-deintercalated having a photoluminescence quantum yield over 20%.

4. Synthesis of 2D GeSn

We are investigating new layered Zintl phase precursors as potential routes to creating 2D GeSn (**Figure 9**). We have synthesized the layered Zintl phase, SrGeSn, as confirmed by pXRD and SEM (**Figure 9a and b**), with the phase consisting of GeSn monolayers (50:50 atomic ratio

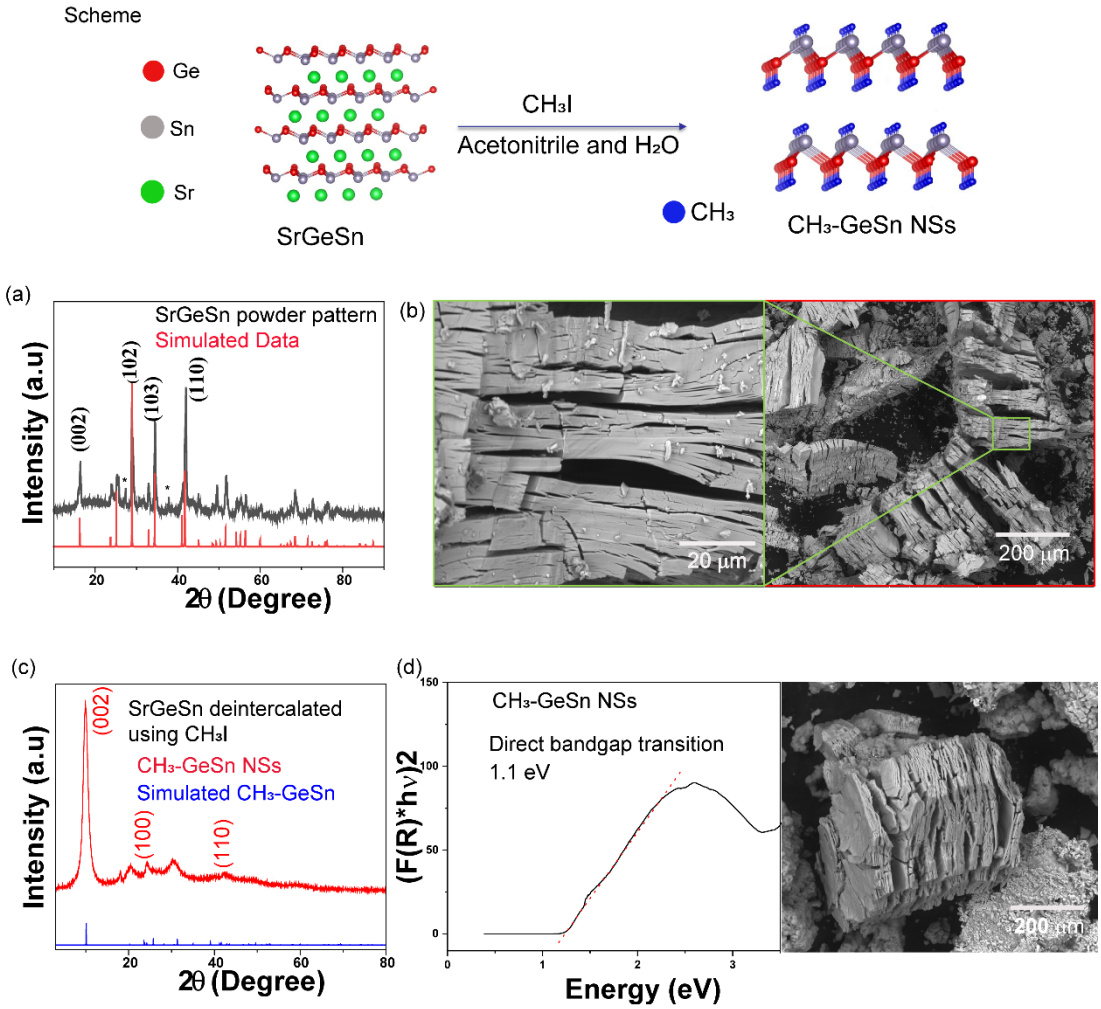

Figure 9. (Scheme) *Crystal structure of SrGeSn Zintl phase and schematic representation of the methyl iodide (CH_3I) deintercaltion yielding 2D CH_3-GeSn.* ***(a)*** *Experimental and simulated pXRD patterns of SrGeSn.* ***(b)*** *SEM images of SrGeSn.* ***(c)*** *Experimental and simulated pXRD patterns of SrGeSn.* ***(d)*** *Tauc analysis of KM-transformed, diffuse reflectance data of the 2D CH_3-GeSn, along with an SEM image on the right.*

Ge:Sn) separated by intercalated Sr atoms (**Figure 9 scheme; top panel**). We have begun exploring pathways to deintercalating this material to form 2D GeSn, guided by our experience with 2D Si and Ge. One pathway that shows promise is using methyl iodide in acetonitrile and water, with the anticipated formation of methyl-terminated 2D GeSn (CH_3-GeSn NSs; **Figure 9 scheme; bottom panel**). pXRD and SEM of the resultant material confirm that (i) Sr is almost fully deintercalated (<3 at.% remaining), (ii) the layered structure is preserved, (iii) the GeSn remains nominally at a 1:1 ratio, with slight Sn enrichment in regions (**Figure 9c and d right panel**; EDX data not shown). The resulting CH_3-GeSn material displays a bandgap of 1.1 eV (1127 nm; **Figure 9d left panel**), consistent with our hypotheses based on the properties of 2D Ge and theoretical works on 2D Sn. Further characterizations are underway to increase our understanding of the structure-property relationships of this material towards optoelectronic applications.

In summary, we have successfully prepared a layered Zintl phase, SrGeSn, and a 2D GeSn material with a bandgap of 1.1 eV and the highest Sn content of all reported 2D GeSn materials. We found that the Zintl phase exists as GeSn monolayers in a 50:50 atomic ratio with intercalated Sr. Deintercalation of Sr with methyl iodide gives a 2D material consisting of nearly 1:1 Ge:Sn with slight Sn enrichment and possessing a bandgap of 1.1 eV. These properties make this material a prime candidate for infrared optoelectronic and thermoelectric applications.

5. Investigation of Lasing in 2D Group IV Semiconductors

Given the strong evidence for band structure engineering in the chlorine-deintercalated material (section 3; **Figure 8**), we have probed this material for optical gain (a prerequisite for lasing) with ultrafast transient absorption. Consistent with our hypotheses, the material displays optical gain (**Figure 10**), a feature that has not yet been observed in other 2D Group IV systems (e.g., hydrogen-terminated 2D Si). Further characterization of the structure-property relationships of this material will direct improvement and optimization of its band structure and luminescent properties to enhance the optical gain towards demonstration of (low-threshold) lasing.

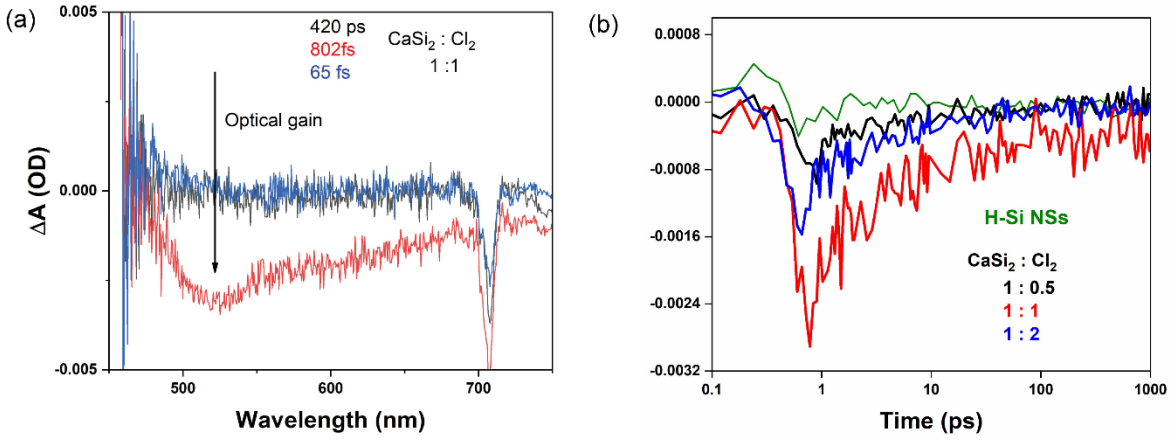

Figure 10. (a) *Transient absorption spectra of the chlorine-deintercalated material (1:1 Cl_2:$CaSi_2$) for three different delay times. (b) Transient absorption decays for the three different chlorine-deintercalated samples, as well as hydrogen-terminated 2D Si sample, for reference.*

In summary, we demonstrated optical gain from a 2D Group IV material for the first time. We found that deintercalating $CaSi_2$ with Cl_2 yields highly luminescent Si nanosheets photoluminescence quantum yields exceeding 20%. Transient absorption studies indicate optical gain.

C. Dissemination of Results

Publications

12 publications in peer-reviewed journals - Funding from this grant resulted in 8 publications, with four additional manuscripts that will be submitted for publication by the end of 2023.

published

1. Ryan, B. J., Roling, L. T., & Panthani, M. G. (2021). Anisotropic Disorder and Thermal Stability of Silicane. *ACS Nano*, *15*(9), 14557-14569.
2. Ferris, M. S., Chesney, A. P., Ryan, B. J., Ramesh, U., Panthani, M. G., & Cash, K. J. (2021). Silicon nanocrystals as signal transducers in ionophore-based fluorescent nanosensors. *Sensors and Actuators B: Chemical*, *331*, 129350.
3. Ryan, B.J., Diroll, B.T., Guo, Y., Dolgos, C.J., Wang, Q.H., Roling, L.T. and Panthani, M.G., (2021). Silicon nanosheets as candidates for silicon-based optoelectronics. ECS Transactions, 102(1), p.3.
4. Hong, S.; Burkhow, S.; Doughhty, R.; Ryan, B.J; Mantravadi, A.; Roling, L.; Panthani, M.G.; Osterloh, F.; Smith, E.A.; Zaikina, J., "Local Structural Disorder in Metavanadates MV_2O_6 Synthesized by Deep Eutectic Solvent Route: Photoactive Oxides with Oxygen Vacancies," (2021) *Chemistry of Materials*, 33(5) 1667-1682.
5. Hadi, A.; Schlichtmann, R.D.; Milot, M.; Slobidsky, J.; Wilsey, M.; Verburg, A.; Chen, Y.; Hamdeh, U.; Ryan, B.J.; Vela, Javier.; Panthani, M.G. "Halide Perovskite Thin Films from a 2D Melt-Processed Precursor," *The Journal of Physical Chemistry Letters* (2023), 14, 22, 5194–5202
6. Sciacca, D.; Berthe, M.; Ryan, B.J.; Peric, N.; Deresmes, D.; Biadala, L.; Boyaval, C.; Addad, A.; Lancry, O.; Makarem, R.; Legendre, S.; Hocrelle, D.; Panthani, M.G.; Prévot, G.; Lhullier, E.; Diener, P.; Grandidier, B., "Transport Properties of methyl-terminated germanane micro-crystallites," (2022) *Nanomaterials.* 12 (7) 1128.
7. Ryan, B.J.; Dorn, R.W.; Essner, J.B.; Bera, A.; Bhaskar, G.; Guo, Y.; Wang, Q.H.; Rossini, A.J.; Zaikina, J.V.; Roling, L.T.; Panthani, M.G., "Luminescent Silicon Nanosheet Paracrystals Synthesized from Elemental and Hydride-derived Precursors: Implications for Photonic and Optoelectronic Applications," *ACS Appl. Nano. Mater* (in press, front cover article)
8. Dorn, R.W.; Ryan, B.J.; Lamahewage, S.N.S.; Dodson, M.V.; Essner, J.B.; Biswas, R.; Panthani, M.G.; Rossini, A.J., "Chlorination of Hydrogenated Silicon Nanosheets Revealed by Solid-State Nuclear Magnetic Resonance Spectroscopy," (2023) *Chem. Mater.* 35 (2) 539-548.

In preparation

9. Essner, J.B.; Bera, A.; Jabrayilov, M.; Chaudhari, A.; Ryan, B.J.; Roling, L.T.; Zaikina, J.V., Panthani, M.G., Two-dimensional Silicon Nanosheets: Effects of Oxidation on Emission
10. Bera, A.; Essner, J.B.; Jabrayilov, M.; Chaudhari, A.; Zaikina, J.V., Panthani, M.G., Abhijit publication on Chlorination
11. Bera, A.; Essner, J.B.; Jabrayilov, M.; Chaudhari, A.; Seymour-Cozzini, T.; Zaikina, J.V., Panthani, M.G. Abhijit publication on GeSn
12. Essner, J.B.; Bera, A.; Jabrayilov, M.; Chaudhari, A.; Zaikina, J.V., Panthani, M.G., Publication on optical gain

Presentations

1. Panthani, M.G., "Group IV Nanosheets with Surface and Composition Tunable Optical Properties," 2023 MRS Spring Meeting. San Francisco, CA. April 2023.

2. Panthani, M.G., "Synthesis and Stability of 2D Silicon Nanosheets," 2022 AIChE Annual Meeting. Phoenix, AZ. Nov 2022.

3. Panthani, M.G., "Synthesis, Structure, and Optical Properties of 2D Group IV Semiconductors," 5th AFRL/ARO/ONR Workshop on GeSn and Related Materials. January 2023. Dayton, OH.

4. Panthani, M.G., "Synthesis, Structure, and Optical Properties of Group IV Semiconductor Nanocrystals and Nanosheets," University of Alabama, Department of Chemistry Seminar Series. Tuscaloosa, AL. April 7, 2022. ***Invited***

5. Panthani, M.G., "Synthesis and Stability of 2D Silicon Nanosheets: A Route to Energy-efficient Computing," Dalhousie University, Clean Energy Institute. Halifax, Nova Scotia (Canada). Sept 29, 2022. ***Invited***

6. Ryan, Bradley J., Benjamin T. Diroll, Yuqi Guo, Carly J. Dolgos, Qing Hua Wang, Luke T. Roling, and Matthew G. Panthani. "Silicon Nanosheets as Candidates for Silicon-Based Optoelectronics." 239th ECS Meeting. May 2021. ***Invited***

7. Panthani, M.G. "Synthesis, Stability, and Optical Properties of Group IV (SiXGeYSnZ) Nanomaterials," 4th AFRL Workshop on GeSn and GeSiSn. September 2021. (Virtual)

8. Panthani, M.G., "Structure, Stability, and Optoelectronic Properties of Silicon Nanomaterials," 2021 AIChE Annual Meeting. Boston, MA. Nov 2021.

D. Changes and Delays

Progress was delayed expected due to challenges in recruiting personnel for this project due to the ongoing COVID-19 pandemic (decrease in applicants, visa restrictions, limited access to research facilities). During 2021 – 2022, the student supported on this research grant was able to finish analyzing data that she had collected prior to the start date of the grant. This student graduated in 2021, leaving a single graduate research assistant in our research lab.

Until March 2022, our research group had a single graduate research assistant. In Spring 2022, we successfully recruited two postdoctoral associates who have made substantial progress in the research objectives.